Journal of Archaeological Science: Reports 14 (2017) 792–799

Contents lists available at ScienceDirect

Journal of Archaeological Science: Reports

journal homepage: www.elsevier.com/locate/jasrep

Orthogonal equations for the detection of hidden archaeological remains de-mystified

Athos Agapiou

Department of Civil Engineering and Geomatics, Faculty of Engineering and Technology, Cyprus University of Technology, 2-6, Saripolou str., 3603 Limassol, Cyprus

ARTICLE INFO

Article history:
Received 28 April 2016
Received in revised form 29 June 2016
Accepted 3 July 2016
Available online 6 July 2016

Keywords:
Orthogonal equations
Crop marks
High resolution images
Remote sensing archaeology
WorlView-2
Stonehenge site

ABSTRACT

Spectral variations of vegetation, known as crop marks, have been widely used for archaeological research as a proxy to detect buried archaeological remains. Such marks can be recognized using space-borne data and image analysis techniques supported by the existing archaeological knowledge of the area under study. Orthogonal equations for the enhancement and detection of crop marks using multispectral satellite images have been recently proposed in the literature. The proposed equations are linear transformations of the initial spectral bands of multispectral datasets aiming to the improvement of the satellite images. For the calculation of the n-space coefficients of this linear transformation a four-step methodology was followed, separately for each sensor. This paper aims to provide the fundamental concept of the development of these equations as well as some aspects related with the application and accuracy assessment. Spectral characteristics of the sensor, atmospheric effects, and spectral calibration of the datasets as well as the selection of the appropriate period for applying these equations for the enhancements of crop marks are also discussed. Such orthogonal equations may be further developed and applied for any kind of sensor either hyperspectral or multispectral for the detection of buried archaeological remains. An example of the applicability of the orthogonal equations at Stonehenge archaeological site is also demonstrated.

1. Introduction

Crop marks have been widely used as a proxy for the exposure of archaeological remains (Gojda and Hejcman, 2012; Alexakis et al., 2009, 2011; Cavalli et al., 2007; Wilgocka et al., 2015; Agapiou et al., 2012). Crop marks are frequently observed in agricultural fields where crops overlay near-surface archaeological remains. The latest tend to retain different percentage of soil moisture compare to cultivate crops that do not cover archaeological remains and therefore the crops can either be stressed or enriched (Winton and Horne, 2010). Consequently, crop marks are formed as an indirect effect of the buried archaeological remains.

The detection of crop marks had attracted the interest of archaeologists especially in the beginning of the 21st century, mainly due to the new capabilities of the satellite and airborne sensors which could provide higher spatial and spectral resolution. However, several researches tend to agree that such marks are difficult to be detected since they constitute a complicated phenomenon (Kaimaris and Patias, 2012). As a result, the recognition of crop marks using remote sensing data is still considered to be extremely challenging.

In the literature a variety of remote sensing techniques are usually applied in satellite datasets for the detection of crop marks. These techniques include amongst other vegetation indices, histogram enhancements, Principal Component Analysis (PCA). Recently, Agapiou et al. (2013a, 2015) have proposed orthogonal equations for a variety of multispectral satellite datasets that can directly applied for the enhancement of multispectral images and therefore the detection of crop marks. In detail, Agapiou et al. (2013a, 2015) have suggested linear equations for QuickBird; IKONOS; WorldView-2; GeoEye-1, ASTER; Landsat 4 TM; Landsat 5 TM and Landsat 7 ETM+ sensors. Further details regarding the orthogonal equations as well as the evaluation report can be found there (Agapiou et al., 2013a, 2015). Although these equations have been initially developed for archaeological sites of the eastern Mediterranean, they have been also exploited in other regions as well (Wilgocka et al., 2015; Rączkowski and Ruciński, 2015; Pagés and Calleja, 2015).

The aim of this paper is twofold: from one hand the paper intends to provide the basic concept and some critical issues related with the applicability of these orthogonal equations, while on the other hand it aims to assist researchers for developing new equations for other kinds of sensors for supporting archaeological research in other areas beyond the eastern Mediterranean. The latest may push further archaeological research to automatic or semi-automatic procedures for the detection of crop marks in vast areas (i.e. archaeolandscapes) and therefore assist archaeological research in a landscape level. In addition,

E-mail address: athos.agapiou@cut.ac.cy.

http://dx.doi.org/10.1016/j.jasrep.2016.07.004

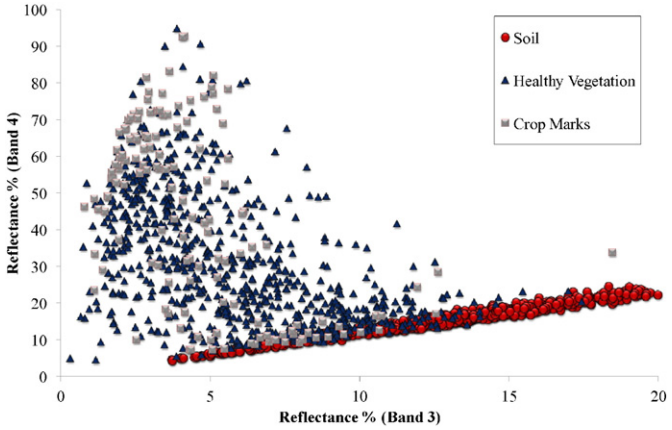

Fig. 1. Reflectance values for the Red and NIR band over the simulated archaeological site (Alampra case study, see Agapiou et al., 2013a, 2013b). The measurements were separated into three main categories: soil spectral signatures; healthy crop spectral signatures and crop marks spectral signature.

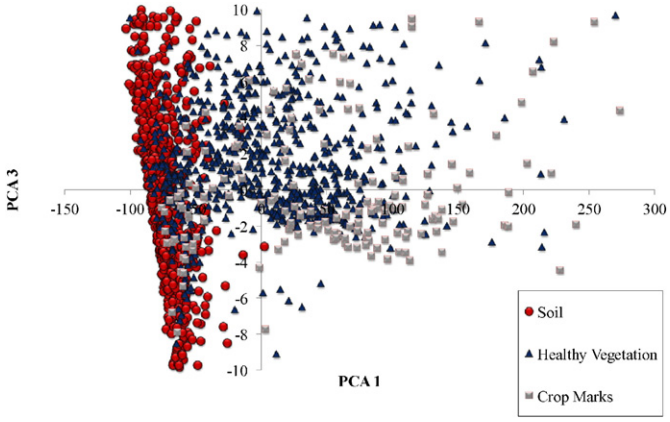

Fig. 2. PCA 1 and PCA 3 components after the transformation of the reflectance values (Alampra case study).

the identification of crop marks which in turn can be linked with the presence of the archaeological remains can be used to protect still unknown and un-excavated cultural heritage sites.

2. Basic concept

The proposed orthogonal equations as those have been proposed by Agapiou et al. (2013a, 2015) have been calculated using a four step methodology -for each sensor- as this is briefly indicated below. It should be noticed that the methodological framework of the work was based upon the fundamental work of Kauth and Thomas (1976) applied for the development of Tasseled-Cap transformation. The basic idea for the development of the new orthogonal equations is to rotate the linear transformation of ground truth datasets after a PCA analysis into a new vector space.

•Step 1: In situ spectral signatures have been systematically collected over simulated archaeological environment using a handheld spectroradiometer (see Agapiou et al., 2013b). The spectral range of the measurements was limited to the visible and infrared part (NIR) of the spectrum (i.e. 450–900 nm) with a span of 1.5 nm interval. Measurements were retrieved during a complete phenological cycle of the crops. Using the appropriate Relative Spectral Response (RSR) filters of each sensor under study (i.e. QuickBird; IKONOS; WorldView-2; GeoEye-1, ASTER; Landsat 4 TM; Landsat 5 TM and Landsat 7 ETM + sensors) the ground hyperspectral measurements have been re-calculated to the appropriate broadband reflectance. Fig. 1 shows the simulation final outcomes for the red and NIR band for Landsat 5 TM sensor after the spectral up-scaling of the ground spectroradiometric measurements. As it is demonstrated, detection of crop marks can be a very difficult task using reflectance values without any post-processing and further analysis of the data. Indeed, crop marks and healthy vegetation tend to give very similar reflectance spectral profiles and therefore their distinction can be problematic.

Table 1
PCA coefficients for the Landsat 5 TM sensor. The first three PCA coefficients could explain more than 99% of the total variance of the data.

	PCA 1	PCA 2	PCA 3	PCA 4
Band 1	−0.076	−0.396	0.304	0.863
Band 2	−0.023	−0.505	0.713	−0.486
Band 3	−0.142	−0.752	−0.630	−0.136
Band 4	0.987	−0.150	−0.051	0.036
Explained	72.83%	24.32%	1.84%	1.02%

•Step 2: Then, the PCA was applied for each dataset for each sensor in order to create the initial eigenspace. PCA was applied to the whole dataset and the first three principal components (PC) have been used. Therefore from the initial four bands of each sensor (B-G-R-NIR) the dataset was limited to three PCs and eigenvectors. The results have shown that the first three components of PCA analysis can explain 99% of the variance of the initial data: PCA 1 = 72.63%; PCA 2 = 25.08%; PCA 3 = 1.43%. The coefficients for the PCA transformation are given in Table 1 for Landsat 5 TM sensor:

Fig. 2 present the new values for Landsat 5 TM after the PCA transformation. As it is shown, soil and vegetation targets (i.e. healthy vegetation and crop marks) can be separated in the 2D space of PCA 1 – PCA 3, while crop marks could then be recognized from the rest of the vegetation especially in the phenophase (time-window) where the crops are photosynthesize.

•Step 3: After the PCs have been defined, the authors have identified three axes in the new 3D space of the dataset (i.e. PC1-PC2-PC3) as following: soil, vegetation and crop marks. The selection of crop marks axes was made upon the best phenophase of the crops, where from previous studies (Agapiou et al., 2013b) it was found to be the most promising period for detection of crop marks. These axes were defined as vectors in this new 3D space with a position vector at the point (0, 0, 0). Then the relative angles between these new axes and the PCs eigenvectors have been calculated.

•Step 4: The final step includes the 3D rotation of the PCA values into the new 3D orthogonal space of the new axes (soil; vegetation; crop marks). The new coefficients have been calculated after a 3D rotation of the eigenvalues based on the relatives angles calculated is Step 3. Therefore new linear coefficients (using the PCA coefficients of Table 1) have been calculated, for the different sensors as indicated for instance for Landsat 5 TM:

$$\begin{aligned} CC1 &= -0.04 * \rho_{\text{Band 1TM}} + 0.02 * \rho_{\text{Band 2TM}} \\ &\quad -0.04 * \rho_{\text{Band 3TM}} + 1.00 * \rho_{\text{Band 4TM}} \\ CC2 &= -0.47 * \rho_{\text{Band 1TM}} - 0.67 * \rho_{\text{Band 2TM}} \\ &\quad -0.57 * \rho_{\text{Band 3TM}} - 0.03 * \rho_{\text{Band 4TM}} \\ CC3 &= 0.19 * \rho_{\text{Band 1TM}} + 0.56 * \rho_{\text{Band 2TM}} \\ &\quad -0.81 * \rho_{\text{Band 3TM}} - 0.04 * \rho_{\text{Band 4TM}} \end{aligned} \quad (1)$$

where CC1 (i.e. Crop Coefficient) corresponds to the vegetation axis; CC2 to soil and CC3 to crop mark axis. Such equations are expected to enhance crop marks, vegetation and soil pixels for each specific sensor

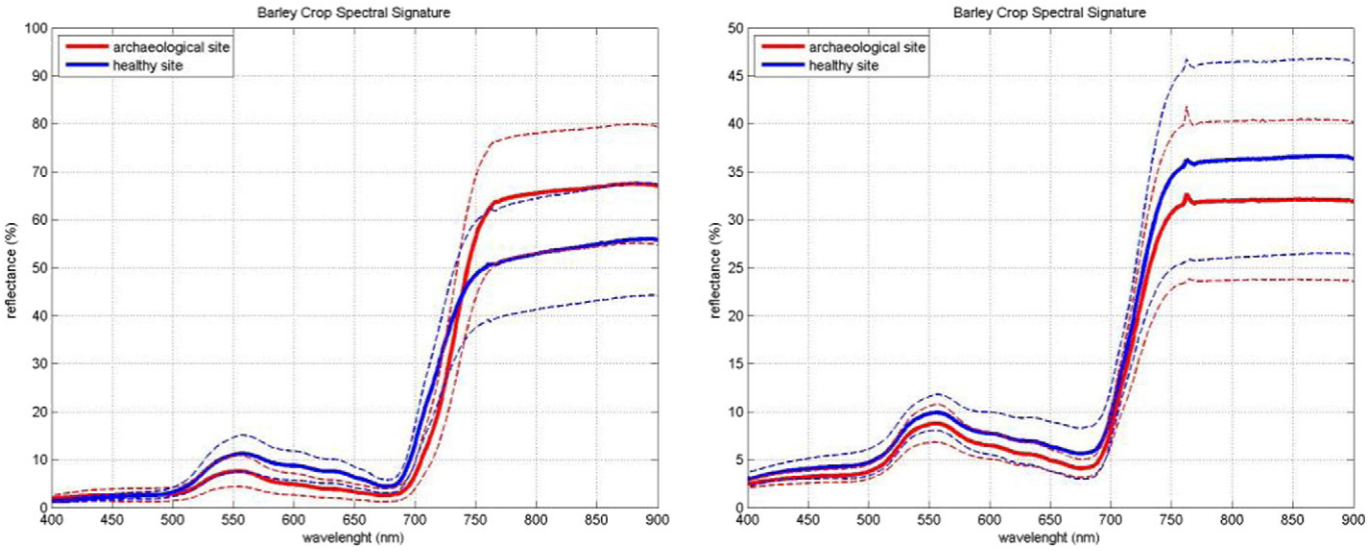

Fig. 3. Spectral profile of crop marks (red line) and healthy cultivated crops (blue line) during the boot stage (left) and prior to the boot stage (right) of the crops. Dash lines indicate the standard deviation of the reflectance (Agapiou et al., 2013b).

selected. The proposed equations have been evaluated in different archaeological sites of Cyprus and Greece (i.e."*Nea Paphos*"; "*Ilis*"; "*Thesallian Plain*") with success. Further details from these applications can be found in Agapiou et al. (2013a, 2015).

3. Spectralconfusion

This section aims to address some important aspects related to the usage and expectations from the above mentioned orthogonal equations. The phenological status, the vegetation type, the spatial resolution of the images, the impact of the atmospheric effects and the spectral characteristics of the satellite sensors used can influence the final results and interpretation.

3.1. Phenological cycle and crop marks

As stated earlier, the detection of crop marks in satellite datasets in not an easy task. This is mainly due to the fact that the spectral profile of the crop marks is quite similar to the rest cultivated crops for a long period during the phenological cycle. Indeed, as it was found from previous studies (Agapiou et al., 2013b), crop marks and healthy crops are quite difficult to be spectrally distinguished especially during the first phenological stages of the crops. The best period for detecting crop marks was found to be during the boot stage (15 days' periods). During this period the spectral signature of the crop marks is statistically significantly different from the rest cultivated field as shown in Fig. 3.

Therefore, the proposed equations should work more efficient when satellite data are available for this period (i.e. boot stage) Fig. 4, indicates the PCA1 and PCA3 feature space during the boot stage of the crops. The reflectance values of crop marks and healthy vegetation can be distinguished after the application of the PCA transformation and further enhanced with the rotation of the data to the new CC axes.

However, the selection of the appropriate datasets during the best phenophase for space observation of crop marks is not usually available. Many times, the satellite data selected for archaeological research are archive images taken over the area of interest in various and different phenological stages. For this reason, the authors have proposed different equations for a specific sensor (Landsat 5 TM) for three periods during the phenological cycle of the crops: (a) Period I: from the seeding period until the crops are fully vegetated (Points B to C in Fig. 5); (b) Period II: until the beginning of the boot stage (Points C to D in Fig. 5) and (c) Period III: until the end of the boot stage (Points D to E in Fig. 5). The authors have followed the same methodology as descripted in Section 2 for Landsat 5 TM sensor. Such approach can be expanded and followed for any other sensors as well.

An example of the variations that observed in different phenological stages can be seen in Fig. 6, indicating the 2D space of CC2 and CC3 (i.e. soil and crop mark axis) for crop marks, vegetation and soil. As it is shown, during period I, soil is spectrally mixed with the vegetation

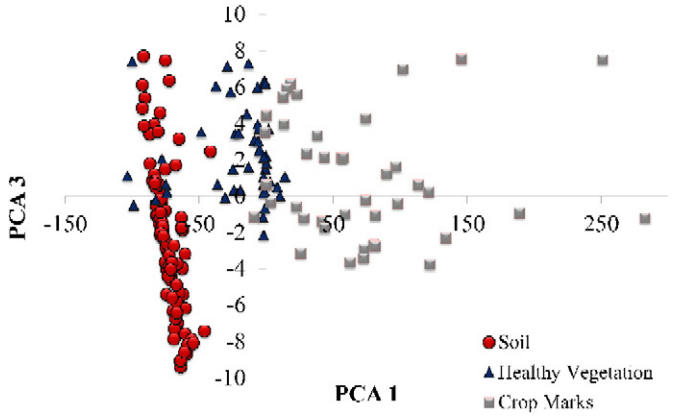

Fig. 4. PCA 1 and PCA 2 components after the transformation of the reflectance values (Alampra case study).

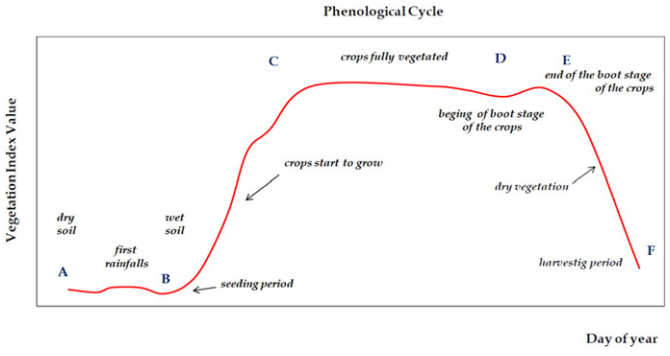

Fig. 5. Phenological cycle of the crops. Important stages of the cycle are indicated in the figure with letters (A to F) while other information regarding the status of the crop is also provided (Agapiou et al., 2013b).

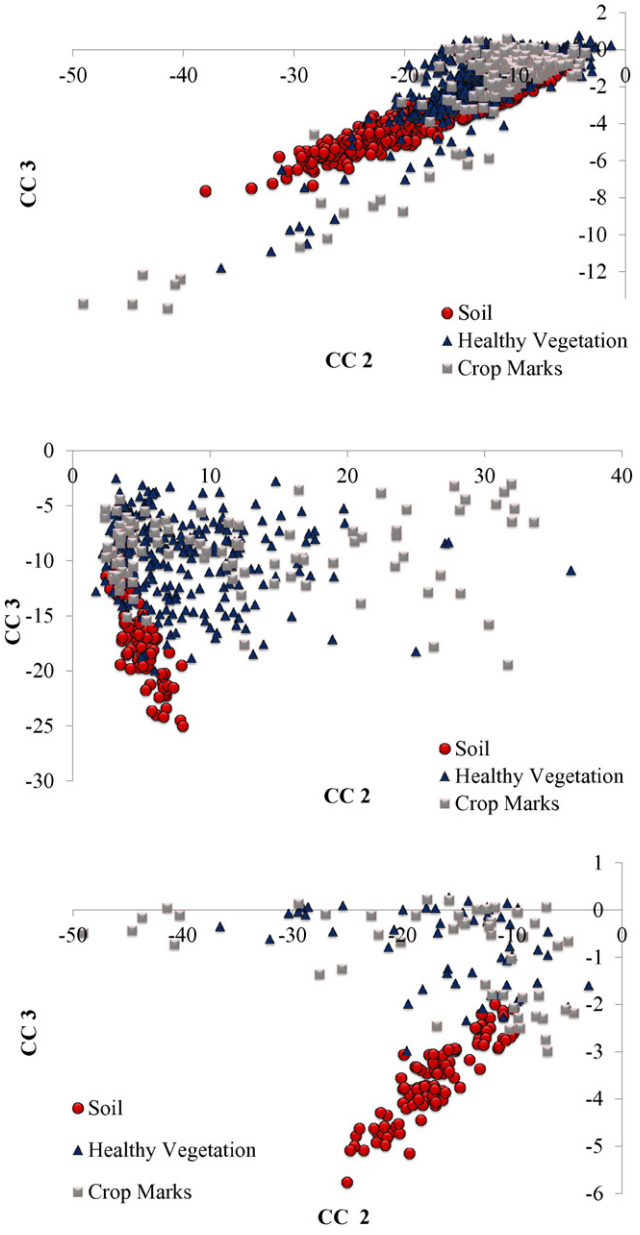

Fig. 6. Soil and Crop mark axis (CC2 and CC3 respectively) applied in three different periods of the phenological cycle: a) from the seeding period until the crops are fully vegetated (Points B to C in Fig. 2); (b) until the beginning of the boot stage (Points C to D in Fig. 2) and (c) until the end of the boot stage (Points D to E in Fig. 2).

and crop mark response. However, during period II and during period III, soil is spectrally separated from the rest of the dataset. In addition, during these periods crop marks are also distinguished from vegetation (healthy cultivated areas), and therefore this can further improve the interpretation of the images.

3.2. Vegetation type and spatial resolution

Additional concerns regarding the proposed equations are related with the type of the vegetation cultivated on the ground surface, on top of the archaeological features. As it was found from previous studies (Agapiou et al., 2013b) both barley and wheat crops tend to provide similar spectral characteristics. However, no other similar study has been contacted for other types of crops or grass by others. Since each type of vegetation is unique, it is expected to give a different spectral profile. Consequently additional equations should be developed specifically designed for these different types of crops. On the other hand, in practice, stress vegetation is expected to behave in the same way for any kind of vegetation (i.e. lower reflectance in the near infrared part of the spectrum) so we might expect to observe similar anomalies in the image. For that reason the proposed equations may also work well for a variety of other types of crops/grasses that have similar spectral characteristics as those initially used for the development of the equations (i.e. barley and wheat crops).

Another critical aspect of the proposed equations is also the spatial resolution of the image used. As it was mentioned earlier, "ground truth" data were used for the development of the proposed equations from ground spectroradiometer. Therefore these equations are designed for "pure" pixels of soil, vegetation and crop marks. These pixels are more likely to be observed in satellite datasets in cultivated areas with high Leaf Area Index (LAI), and therefore have an almost complete coverage with vegetation of the area under examination. In any other case that the crops are not fully vegetated and the area is not fully covered with vegetation or even not fully cultivated, the phenomenon of the mixed pixels might be seen. Consequently, the proposed equations might not work well, when spatial resolution (pixel size) of the satellite sensor is not enough to distinguish crop marks from the background. In

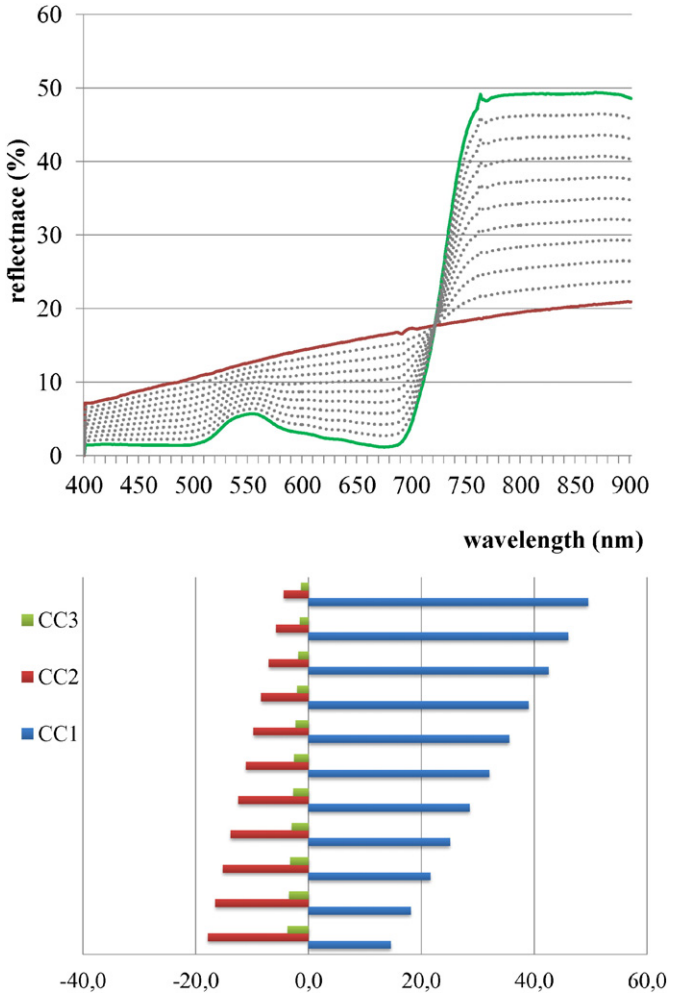

Fig. 7. Spectral profile of vegetation (green line) and soil (red line). Dashed lines indicate the spectral profile of mixed pixels (e.g. 90% of vegetation and 10% of soil) for different levels (top). The results after the application of the orthogonal equations for the vegetation (CC1); soil (CC2) and crop marks (CC3) axis (bottom). The calculation of these new spectral profiles was based on constrained linear un-mixing technique.

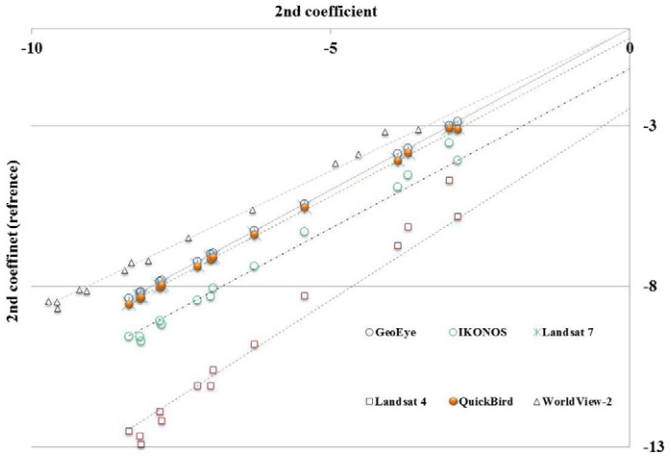

Fig. 8. Linear coefficients of the orthogonal equations for different sensors. GeoEye sensor was used as reference sensor.

this case "pure" elements are "mixed" in the satellite image and therefore a "mixed" pixel (mi-xel) is recorded.

Fig. 7 (top) indicates the spectral behaviour of mixed pixels (with dashed lines) compared to pure vegetation (green line) and soil (red line) targets. The calculation of these simulated spectral profiles was based upon linear constrained spectral un-mixing technique (Ritter and Urcid, 2011). As it is demonstrated the coverage of vegetation (i.e. high LAI index) is essential in order to have "truth" spectral behaviour of the vegetation. Fig. 7 (bottom), indicates the results for the soil; vegetation and crop mark axis after the application of the orthogonal equations for "pure" vegetation target, as well as mixed with soil in different percentages.

3.3. Atmospheric effects and spectral characteristics of the sensor

The orthogonal equations should be applied in radiometric corrected images. Therefore the digital numbers of the image need to be converted into radiance based on the calibration files of each image (i.e. metadata file). Moreover, radiance to reflectance correction is needed. At this

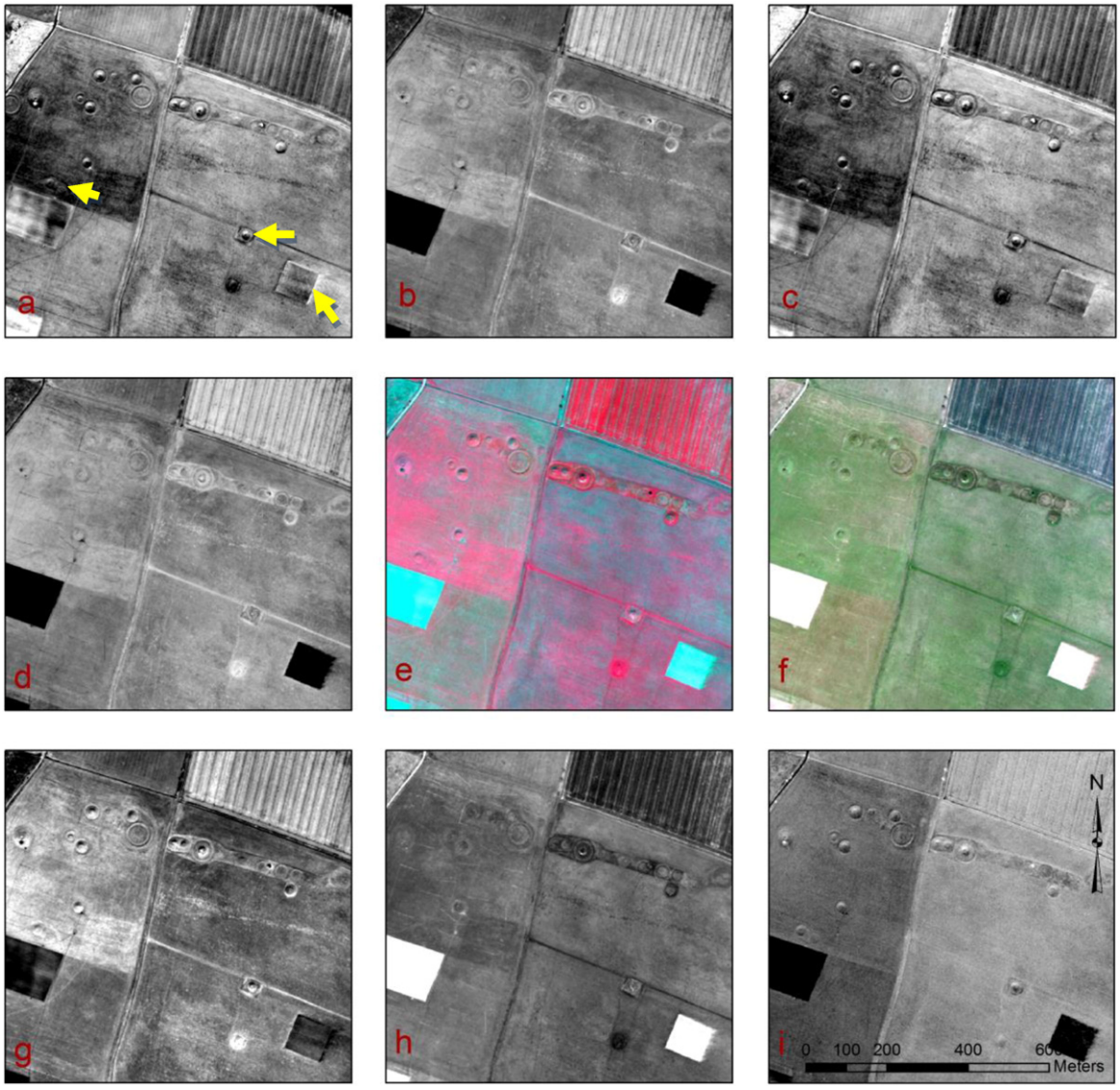

Fig. 9. The prehistoric landscape of Stonehenge as recorded from WorkdView-2 after the application of the orthogonal equations by crop component (a); vegetation component (b); soil component (c); NDVI index (d); NIR-R-G (e); R-G-B (f); 1st PC (g); 2nd PC (h) and 3rd PC (i).

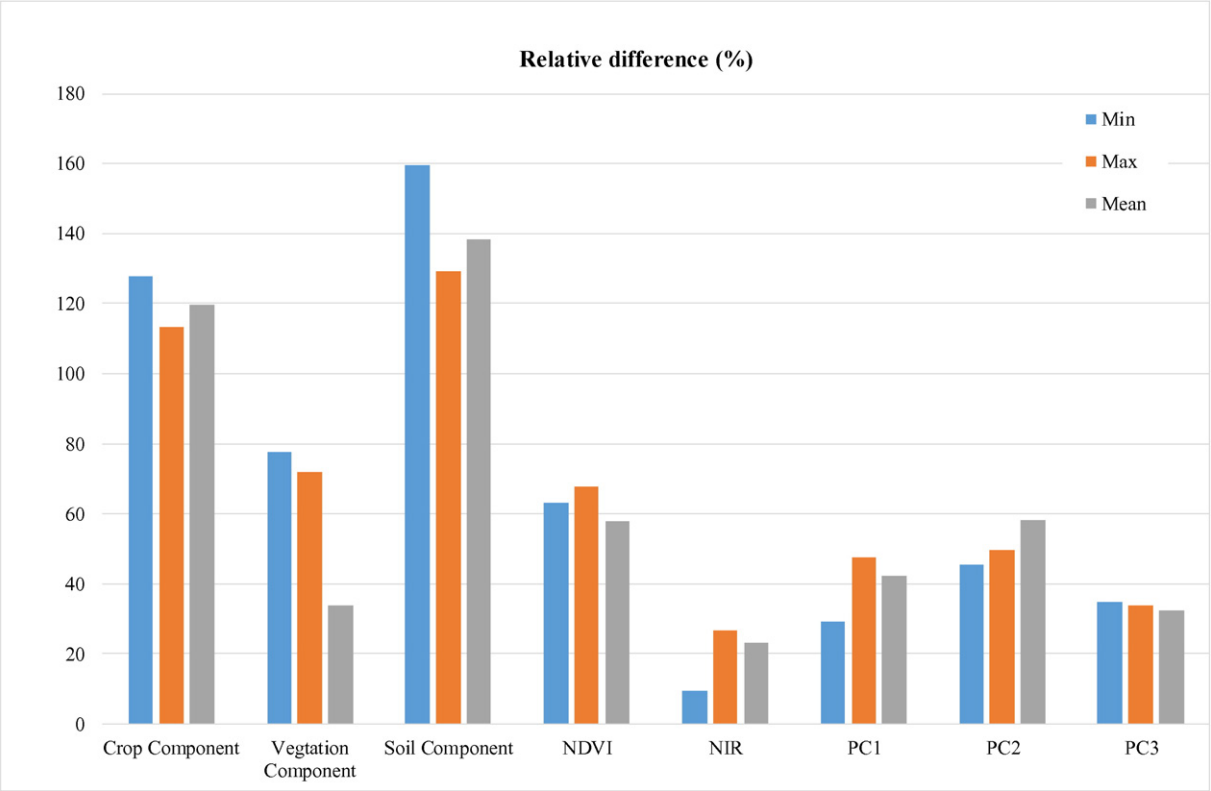

Fig. 10. Relative difference between "crop marks" and "vegetated" areas for different algorithms applied in the case study of Stonehenge.

stage it is very important to evaluate and correct the atmospheric conditions of the image at the time of acquisition. Atmospheric effects such as scattering and absorption can also influence the final results after the application of orthogonal equations. The removal of the atmospheric effects is an important pre-processing step required in many remote sensing applications, since it is needed to convert the at-satellite spectral radiances of satellite imagery to their at-surface counterparts (Bastiaanssen et al., 2000; Kaufman and Sendra, 1988).

Atmospheric effects for both spectral signatures as well as for vegetation indices have been discussed in the literature since the 1980s (Duggin and Piwinski, 1984). Atmosphere is a principal source of noise in all applications of optical remote sensing using satellite datasets. These errors, caused by atmospheric effects, can increase the uncertainty of the final results up to 10%, depending on the spectral band under investigation. Recently Hadjimitsis et al. (2010) has highlighted that non atmospheric correction of the satellite data can even increase the inaccuracy of several vegetation indices such as the NDVI. This uncertainty might reach up to 18%. In another study (Agapiou et al., 2011) the mean differences of 15% between the atmospheric and non-atmospheric corrected values for NDVI index have been also recorded.

Satellite sensors have similar spectral characteristics but these are not exactly identical. Since the spectral characteristics of each sensor are different due to different RSR filters, orthogonal equations had calculated separately for each sensor. Fig. 8 presents the variations of the linear coefficients for the crop mark component. The GeoEye sensor was selected as the reference line. As it is indicated similar spectral response it is expected between the sensors but some difference still exists. Variations between the Landsat sensors (7 ETM+ and 4 TM) are also recorded. These dissimilarities are also known from previous studies indicating the spectral resolution and the spectral characteristics of the sensors (Agapiou et al., 2014).

4. Applications of orthogonal equations

In order to evaluate the orthogonal equations in other areas beyond the Mediterranean region, we have tested them in the well-known prehistoric landscape of Stonehenge (UK). The site -a UNESCO World Heritage monument- was selected since here the first known photograph from above using a balloon was taken in 1906 by Lieutenant Philip Henry Sharpe of the Royal Engineers' Balloon Section, marking -in a way- the beginning of what is known today as "remote sensing archaeology". The site has attracted the interest of many researchers over the years while remote sensing applications have been already contacted in this landscape (e.g. De Smedt et al., 2014; Pearson, 2015).

Two different datasets have been used as an example of the applicability of the proposed orthogonal equations. One very high resolution WorldView-2 image (overpass at 2015-04-09) with spatial resolution of 2 m and one medium resolution Landsat 5 TM (overpass at 2011-09-28) with spatial resolution of 30 m were used. Fig. 9 presents the results of the orthogonal equations (a–c) as well as the NDVI and pseudo colour composites applied in the WorldView-2 image. In addition the first three principal components are shown in Fig. 9g–i. As it is demonstrated by the results visual interpretation can be improved for the exposure of crop marks after the application of the orthogonal equations especially in the vegetation component application. It is important to see also the improvements of the image in areas that tend to give low NDVI values (Fig. 9d black squares). In these areas both crop and soil component (Fig. 9a and c) can enhance the initial image indicating the boundaries of these areas in contrary to NDVI and pseudo colour composites (Fig. 8d–f). Some crop marks that are difficult to be observed in these images and are improved after the application of the orthogonal equations are indicated with arrow in Fig. 9a. The 1st PC (Fig. 9g) is able also to enhance the crop marks in this area compare to the rest of the PCs (Fig. 9h–i). PCA analysis has been proven to be able to enhance

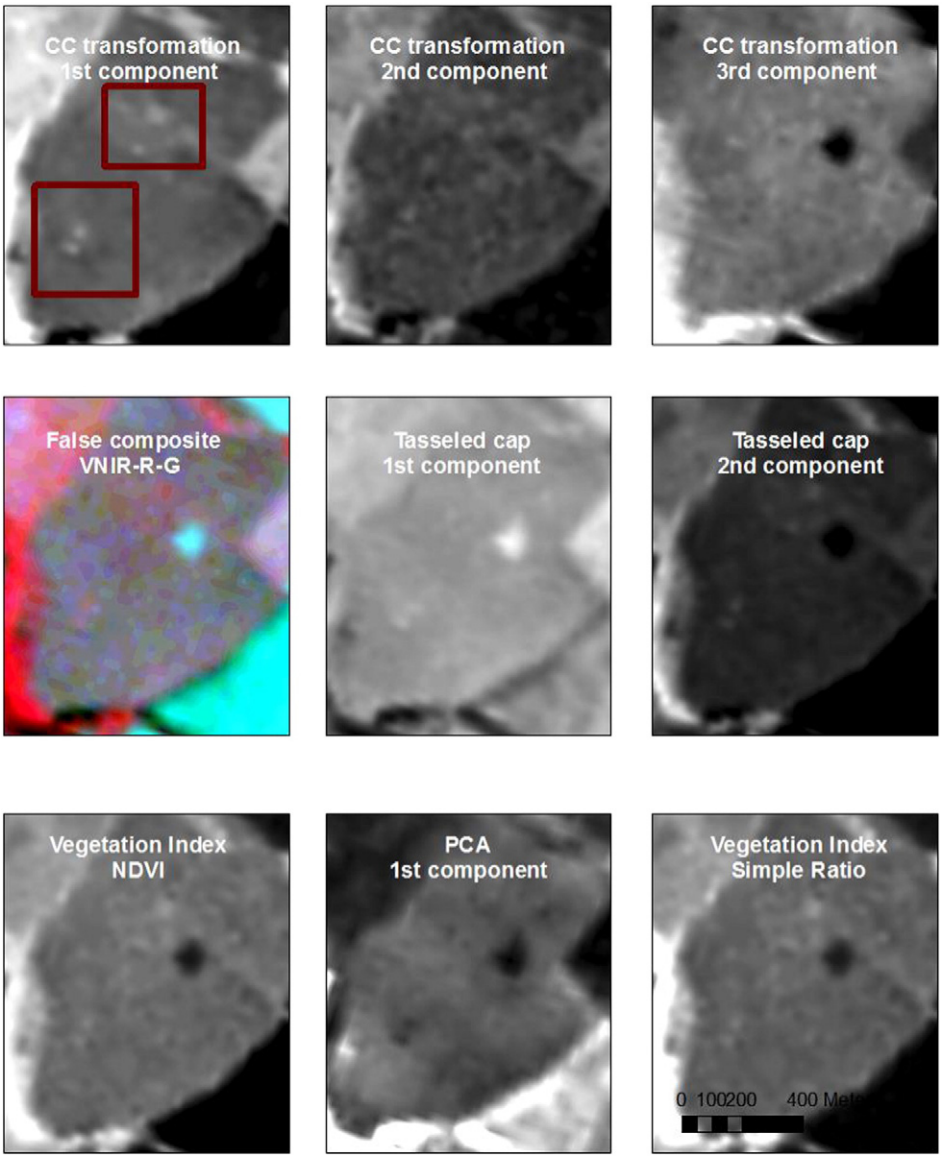

Fig. 11. The prehistoric landscape of Stonehenge as recorded from Landsat 5 TM from orthogonal equations, vegetation indices, PCA analysis, and Tasseled cap transformations.

and improve the raw images although in some cases from previous studies PCA can over-saturate the image under investigation (Agapiou et al., 2013a).

Quantitative analysis for the above mentioned algorithms in order to examine their performance for the enhancement of crop marks is presented in Fig. 10. For the estimation of this analysis more than 500 points have been collected from the image both from areas characterized as "crop marks" as well from the rest "vegetated" areas. Then the values where normalized based in their standard deviation and finally their relative difference was calculated. As it is demonstrated crop and soil component where able to enhance more than 100% the relative difference between crop marks and the vegetated areas. In general all the algorithms were able to enhance the image (i.e. more than 20% relative difference).

Results from the medium resolution of Landsat 5 in the same archaeological site are demonstrated in Fig. 11. In spite of the poor results that are recorded mainly due to the spatial resolution of the image, some "anomalies" can be seen in the image after the application of the crop mark component (Fig. 11, red squares). Even though the improvements of the technology regarding the space sensors and the improvements seen in the spatial resolution of multispectral images, the Landsat series still remains a very important dataset due to the fact that can provide systematic data since 1972. Therefore, orthogonal equations can be used in these datasets as well (using the appropriate coefficients) in an attempt to recover useful information for the landscape of an area. Vegetation indices and false composites do not improve any further the initial image highlighting the difficulties that many researchers affront in working with an "unknown" landscape. Tasseled cap and PCA analysis were able to enhance some of the crop marks in the Landsat image but in all cases the results but with some problematic aspects as well (i.e. over saturation of the initial image). For instance, PCA analysis was able to detect the southern crop mark only while the results from the 1st component of Tasseled cap exhibit the low Signal-to-Noise Ratio (SNR) and therefore hinders the interpretation of the data. In the case of the crop component the crop marks were able to be detected as indicated in the Fig. 11. Of course the spatial resolution of the image prohibits the detail recognition of the crop marks as in the first case of WorldView-2 case study.

5. Conclusions

This paper aims to present the applicability of orthogonal equations for the detection of crop marks in areas beyond the eastern Mediterranean region. These equations have been recently proposed in the literature in an effort to intensify crop marks through interpretation of multispectral satellite datasets.

Further to the utility of the proposed orthogonal equations and their testing in different archaeological environments, the paper highlights some limitations and quotes some considerations regarding the usability of these equations, including the impact of atmospheric effects, the phenological stage of the crops as well as the characteristics of the sensors. Two examples using both high and medium resolution satellite images in the case study of Stonehenge are also presented.

It should be mentioned however that detection and interpretation of crop marks is not necessarily related to the detection of archaeological remains. Crop marks are currently used as a proxy for the detection of buried archaeological features which can be confirmed only after an in-situ archaeological investigation and excavation. However, studying and analysing crop marks though satellite datasets, allows archaeologists and researchers to examine in large areas the archaeolandscape and to identify possible potential "interesting" areas that are worthy of further investigations and/or protection.

Future study is expected to carry out for improving the orthogonal equations by minimizing atmospheric effects (i.e. atmospheric resistance orthogonal equations) and also minimizing phenological variations.

Acknowledgments

The present communication is under the "ATHENA" project H2020-TWINN2015 of European Commission. This project has received funding from the European Union's Horizon 2020 research and innovation programme under grant agreement No 691936. Thanks are also given to the Remote Sensing and Geo-environment Research Laboratory of the Department of Civil Engineering & Geomatics of the Cyprus University of Technology for the support (http://www.cut.ac.cy).

References

Agapiou, A., Alexakis, D., Hadjimitsis, D.G., 2014. Evaluation of spectral sensitivity of ALOS, ASTER, IKONOS, LANDSAT and SPOT satellite sensors intended for the detection of archaeological crop marks. Int. J. Digital Earth 7 (5). http://dx.doi.org/10.1080/17538947.2012.674159.

Agapiou, A., Alexakis, D.D., Sarris, A., Hadjimitsis, D.G., 2013a. Orthogonal re-projection of spectral bands using medium and high resolution satellite images for the detection of archaeological crop marks. Remote Sens. 5 (12), 6560–6586. http://dx.doi.org/10.3390/rs5126560.

Agapiou, A., Alexakis, D.D., Sarris, A., Hadjimitsis, D.G., 2015. Linear 3-D transformations of Landsat 5 TM satellite images for the enhancement of archaeological signatures during the phenological of crops. Int. J. Remote Sens. 36 (1), 20–35.

Agapiou, A., Hadjimitsis, D.G., Alexakis, D., Papadavid, G., 2012. Examining the phenological cycle of barley (*Hordeum vulgare*) using satellite and in situ spectroradiometer measurements for the detection of buried archaeological remains. GISci. Remote. Sens. 49 (6), 854–872.

Agapiou, A., Hadjimitsis, D.G., Papoutsa, C., Alexakis, D.D., Papadavid, G., 2011. The importance of accounting for atmospheric effects in the application of NDVI and interpretation of satellite imagery supporting archaeological research: the case studies of Palaepaphos and Nea Paphos sites in Cyprus. Remote Sens. 3 (12), 2605–2629.

Agapiou, A., Hadjimitsis, D.G., Sarris, A., Georgopoulos, A., Alexakis, D.D., 2013b. Optimum temporal and spectral window for monitoring crop marks over archaeological remains in the Mediterranean region. J. Archaeol. Sci. 40 (3), 1479–1492. http://dx.doi.org/10.1016/j.jas.2012.10.036.

Alexakis, A., Sarris, A., Astaras, T., Albanakis, K., 2009. Detection of neolithic settlements in Thessaly (Greece) through multispectral and hyperspectral satellite imagery. Sensors 9, 1167–1187.

Alexakis, A., Sarris, A., Astaras, T., Albanakis, K., 2011. Integrated GIS, remote sensing and geomorphologic approaches for the reconstruction of the landscape habitation of Thessaly during the neolithic period. J. Archaeol. Sci. 38, 89–100.

Bastiaanssen, W.G.M., Molden, D.J., Makin, I.W., 2000. Remote sensing for irrigated agriculture: examples from research and possible applications. Agric. Water Manag. 2000 (46), 137–155.

Cavalli, R.S., Colosi, F., Palombo, A., Pignatti, S., Poscolieri, M., 2007. Remote hyperspectral imagery as a support to archaeological prospection. J. Cult. Herit. 8, 272–283.

De Smedt, P., Van Meirvenne, M., Saey, T., Baldwin, E., Gaffney, C., Gaffney, V., 2014. Unveiling the prehistoric landscape at Stonehenge through multi-receiver EMI. J. Archaeol. Sci. 50, 16–23.

Duggin, M.J., Piwinski, D., 1984. Recorded radiance indices for vegetation monitoring using NOAA AVHRR data; atmospheric and other effects in multitemporal data sets. Appl. Opt. 1984 (23), 2620–2623.

Gojda, M., Hejcman, M., 2012. Cropmarks in main field crops enable the identification of a wide spectrum of buried features on archaeological sites in Central Europe. Journal of Archaeological Science 39 (6), 1655–1664 (ISSN 0305-4403, 10.1016/j.jas.2012.01.023).

Hadjimitsis, D.G., Papadavid, G., Agapiou, A., Themistocleous, K., Hadjimitsis, M.G., Retalis, A., Michaelides, S., Chrysoulakis, N., Toulios, L., Clayton, C.R.I., 2010. Atmospheric correction for satellite remotely sensed data intended for agricultural applications: impact on vegetation indices. Nat. Hazards Earth Syst. Sci. 2010 (10), 89–95. http://dx.doi.org/10.5194/nhess-10-89-2010.

Kaimaris, D., Patias, P., 2012. Best period for high spatial resolution satellite images for the detection of marks of buried structures. Egypt. J. Remote Sens. Space. Sci. (ISSN 1110-9823, 10.1016/j.ejrs.2011.12.001).

Kaufman, Y.J., Sendra, C., 1988. Algorithm for automatic corrections to visible and near-IR satellite imagery. Int. J. Remote Sens. 1988 (9), 1357–1381.

Kauth, J.R., Thomas, S.G., 1976. The tasseled cap - a graphic description of the spectral-temporal development of agricultural crops as seen by LANDSAT. Proc. Symposium on Machine Processing of Remotely Sensed Data 4B. Purdue University of West Lafayette, Indiana, pp. 44–51.

Pagés, O.R., Calleja, J.F., 2015. Remote sensing for archaeological studies and territory management: case study of the Roman city of Lucas Asturum (Asturias, Spain). Proceeding of the Workshop Advances in Remote Sensing for Cultural Heritage: From Site Detection, to Documentation and Risk Monitoring, 12–13 November 2015 - ESA - ESRIN, Frascati (Rome), Italy.

Pearson, P.M., 2015. The sarsen stones of Stonehenge. Proc. Geol. Assoc. http://dx.doi.org/10.1016/j.pgeola.2015.07.004.

Rączkowski, W., Ruciński, D., 2015. Searching for hidden houses: optical satellite imagery in archaeological prospection of the early Neolithic settlements in the Kujawy Region, Poland. Proc. SPIE 9535, 95350V.

Ritter, X.G., Urcid, G., 2011. A lattice matrix method for hyperspectral image unmixing. Inf. Sci. 181 (10), 1787–1803.

Wilgocka, A., Ruciński, D., Rączkowskia, W., 2015. Romantic versus scientific perspective: the ruins of Radlin palace in Wielkopolska Region in the light of remote sensing techniques. Proc. SPIE 9535, 95350W. http://dx.doi.org/10.1117/12.2195594.

Winton, H., Horne, P., 2010. National archives for national survey programmes: NMP and the English heritage aerial photograph collection. Landscapes through the Lens. Aerial Photographs and Historic Enviroment. Aerial Archaeology Research Group No. 2, pp. 7–18.